Carbon 157 (2020) 602–613

Contents lists available at ScienceDirect

Carbon

journal homepage: www.elsevier.com/locate/carbon

Enhancement of the strength-ductility relationship for carbon nanotube/Al–Cu–Mg nanocomposites by material parameter optimisation

Z.Y. Liu [a], K. Ma [a], G.H. Fan [b], K. Zhao [a], J.F. Zhang [a], B.L. Xiao [a, *], Z.Y. Ma [a, **]

[a] Shenyang National Laboratory for Materials Science, Institute of Metal Research, Chinese Academy of Sciences, 72 Wenhua Road, Shenyang, 110016, China
[b] School of Materials Science and Engineering, Harbin Institute of Technology, Harbin, 150001, China

ARTICLE INFO

Article history:
Received 7 August 2019
Received in revised form
27 October 2019
Accepted 28 October 2019
Available online 31 October 2019

ABSTRACT

Heterogeneous carbon nanotube (CNT)/Al–Cu–Mg composites, consisting of CNT-free coarse grain (CG) bands and CNT-rich ultrafine grain (UFG) zones, were fabricated to significantly enhance their strength-ductility. Their mechanical behavior as well as extra-strengthening and elongation increase mechanisms were investigated in detail, with the help of high-resolution digital image correlation (DIC) and extended finite element method (XFEM). A narrow CG band and medium CG content were found to be beneficial in increasing the strength-ductility. Under optimized conditions, a heterogeneous 3 vol% CNT/Al composite exhibited more than 100% elongation increase with nearly no ultimate tensile strength loss as compared to the uniform composite. Geometrically necessary dislocations were induced between the CG and UFG zones, leading to extra-strengthening beyond the rule-of-mixtures. Local strain and micro-crack propagation analyses based on DIC and XFEM indicated that strain localization was greatly suppressed and micro-cracks were effectively blunted because of the existence of CG bands, leading to considerably enhanced elongation. Finally, a model was proposed to assist the selection of the heterogeneous structure parameters for the strength-ductility design of the nanocomposite. The calculated safety zones for CG parameter selection were in well agreement with the experimental results.

1. Introduction

Carbon nanotubes (CNTs) have extremely high strength (approximately 30 GPa) and elastic modulus (approximately 1 TPa) [1–3]. Therefore, they are considered as ideal reinforcements for aluminum alloys. In the past decade, various fabrication methods for CNT-reinforced aluminum (CNT/Al) composites have been investigated [4–13], including friction stir processing [6], molecular level mixing [7], and high-energy ball milling (HEBM) [10–13]. As expected, CNTs exhibited extraordinary strengthening effects on the aluminum matrix [5,8], and various strengthening mechanisms have been suggested [14,15]. One particular mechanism is the strengthening resulting from CNT-stabilized ultrafine grains (UFGs) formed during fabrication, e.g., HEBM [15].

Because of the UFGs and pinning effect on dislocations due to CNTs, the strengthening of the CNT/Al composites is usually accompanied by a considerable ductility loss, limiting their engineering application. To overcome this issue, flaky powder metallurgy and interface bonding modification have been adopted to obtain enhanced ductility [16–18]. Recently, the heterogeneous structure design with inhomogeneous distribution of reinforcements or grain sizes was also demonstrated to be a potentially effective way of improving the strength-ductility of UFG metals or composites [19–23]. For example, Vajpai et al. [24] and Ota et al. [25] constructed 3-D gradient harmonic grain structures in pure Al, pure Ti, Ti–6Al–4V, and stainless steel using milling-sintering routes. It was found that, compared to coarse grain structure, 3-D gradient harmonic grain structure led to significant strength and toughness enhancements by avoiding strain localization during plastic deformation. A similar phenomenon was also found for composites, e.g., the strength and ductility of the nano-sized B_4C/Al composite with a heterogeneous structure were found to be simultaneously increased as compared to that of the uniform composite [22].

Although enhanced strength-ductility was reported in

* Corresponding author.
** Corresponding author.
E-mail addresses: blxiao@imr.ac.cn (B.L. Xiao), zyma@imr.ac.cn (Z.Y. Ma).

https://doi.org/10.1016/j.carbon.2019.10.080
0008-6223/

heterogeneous composites reinforced with micro-sized particles, e.g., B_4Cp/Al, TiB_w/Ti composites, in the past few years [26,27], little attention has been paid to the toughening of heterogeneous CNT/Al composites. To the best of our knowledge, only two investigations for increasing the strength-ductility of CNT/Al composites in this strategy have been reported [28,29]. Wei et al. [28] achieved increased strength in CNT/7055Al composites by introducing 7055Al flaky powders. However, the principle of the microstructure optimisation was not mentioned. Salama et al. [29] tried to introduce ductile zones without CNTs in brittle CNT/Al composites. However, the strength-ductility enhancement was not pronounced due to the interfacial separation of ductile-brittle zones. Therefore, it is worthwhile to investigate in depth the toughening behavior of the heterogeneous CNT/Al composites.

In this study, we developed a method for fabricating heterogeneous CNT/Al composites with inhomogeneous distribution of CNTs as well as grains. CNT-free coarse grain (CG) bands were introduced into the UFG CNT/Al composites by the conventional powder metallurgy (PM) route. The aim is to (a) develop CNT/Al composites with much higher strength-ductility through the heterogeneous structure design, (b) clarify the toughening mechanism of the heterogeneous structure, and (c) propose a model for structure parameter selection of heterogeneous nanocomposites.

2. Experimental

In this study, composites with both heterogeneous and uniform structures were fabricated through HEBM and PM routes as shown in Fig. 1. Atomized 2009Al (Al-4 wt.% Cu-1.5 wt% Mg) powders with approximately 10 μm diameters were used as raw materials. CNTs (~98% purity) fabricated by chemical vapor deposition in Tsinghua University had an outer diameter of 10–30 nm and a length of ~5 μm. No extra pretreatment was conducted on CNTs.

CNTs were ball milled with 10 μm as-received 2009Al powders at a rotation rate of 400 rpm and with a ball-to-powder ratio of 15:1 for 6 h using an attritor. The ball-milled powders were then mixed with the as-received 2009Al powders with different average sizes (30, 10, and 2 μm) and volume fractions using a dual-axis mixer at a rotation rate of 50 rpm for 6 h, thereby obtaining composite powders for the fabrication of the heterogeneous composites with different local CNT concentrations and CG structures. For comparison, the as-mixed 2009Al powders as well as the as-milled CNT/2009Al composite powders were prepared.

The composite powders were cold compacted and then vacuum hot pressed into billets under a pressure of 50 MPa at 833 K. The billets were extruded into bars at 703 K with an extrusion ratio of 16:1. The extruded bars were solution treated at 770 K for 2 h,

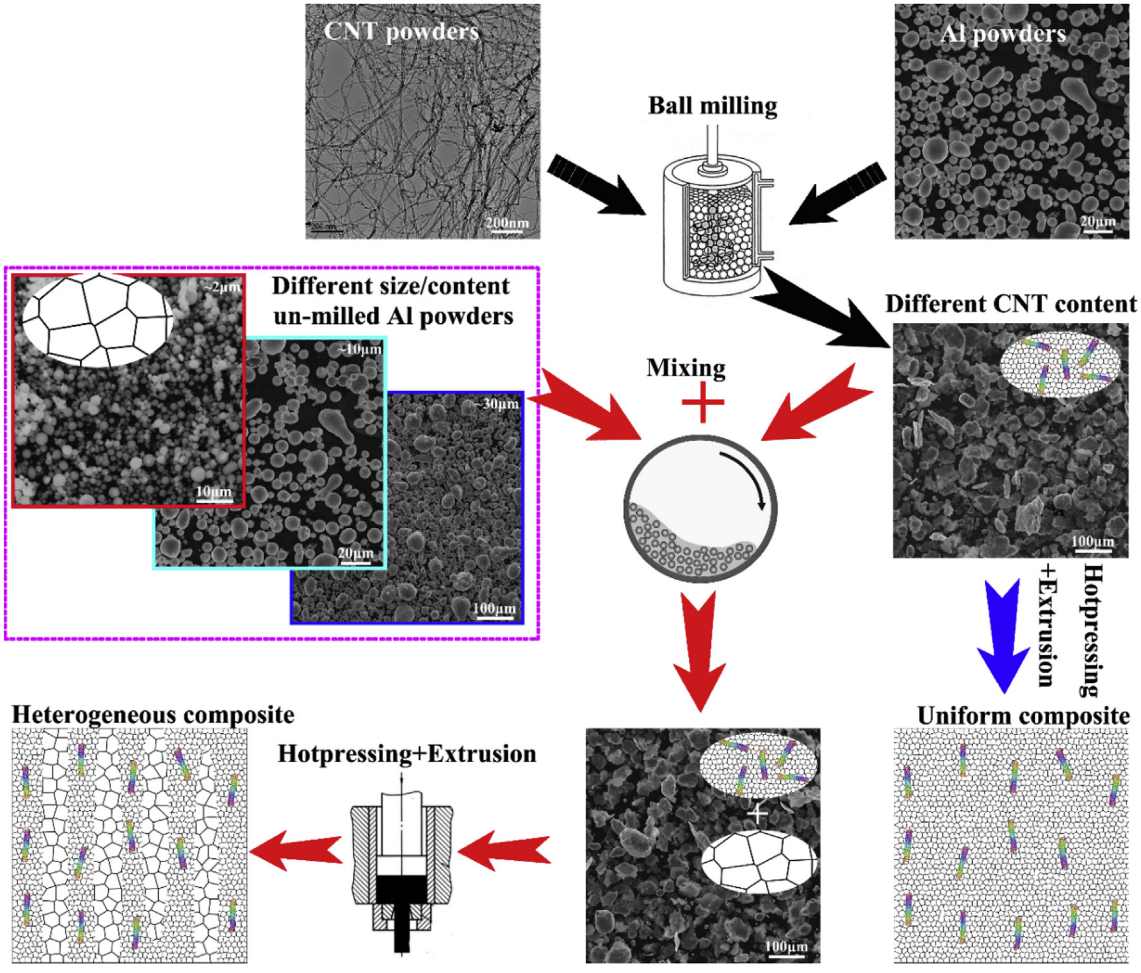

Fig. 1. Schematic of the fabrication process of CNT/2009Al composites with a heterogeneous and uniform structure. (A colour version of this figure can be viewed online.)

quenched into water, and naturally aged for 4 days. For convenience, the heterogeneous composites obtained by mixing the as-milled A vol% CNT/2009Al composite powders and the as-received B vol% 2009Al alloy powders with large, small, and ultra-fine sizes were, respectively, abbreviated as A% CNT-(wide, narrow, or ultra-narrow) B% CG.

Tensile specimens with a gauge diameter of 5 mm and a length of 30 mm were machined from the extruded bars with the axis parallel to the extrusion direction. Tensile tests were carried out at a strain rate of 10^{-3} s^{-1} using an Instron 8862 tester. At least three specimens were tested for each composite. An optical microscope (OM; Zeiss Axiovert 200MAT) and a transmission electron microscope (TEM; Tecnai G2 20) were used to examine the grains and CNT distributions. The powders and fracture surfaces of the tensile specimens were observed using a field-emission scanning electron microscope (FESEM, SUPRA 55). The tensile specimens of the heterogeneous 3 vol% CNT/2009Al composite (4% CNT-25% narrow CG) were interrupted after stretching to different plastic strains and then subjected to SEM or TEM analyses.

An in situ quasi-static micro-tensile stage (Kammrath & Weiss GmbH, Germany) was set up in an FEI SEM (HELIOS Nanolab-600i). Deformation was carried out by uniaxial tensile loading to different levels at a displacement rate of 2 μm/s, and the specimen geometries were 2 mm thick, 2 mm wide, and 18 mm long. Digital images were taken under 4000 × magnification after each strain increment. Commercial VIC-2D software was utilized for digital image correlation (DIC) analysis and the calculation of local strain fields.

An extended finite element method (XFEM) model was built to show the crack blunting effect of CG bands in the heterogeneous composites. A preexisting crack was embedded in UFG zones reinforced by CNTs in both heterogeneous and uniform composites. Tensile loading to 0.75% strain was applied on this model. The linear work hardening equation was used to model the plastic properties of the CG and UFG zones, which follows $\sigma = \sigma_y + M\varepsilon_p$ (where σ_y is the yield stress, M is the strength coefficient, and ε_p is the plastic strain). Young's modulus, maximum principal stress (σ_{mp}) for damage, and all the plastic parameters were determined from tensile loading tests.

3. Results

3.1. Microstructure of heterogeneous composites

Fig. 2 shows the OM images of the heterogeneous 3 vol% CNT/2009Al composites with different CG band widths. An inhomogeneous structure could be observed. The CG bands and the UFG zones were observed as bright and dark regions, respectively, because of the higher susceptibility of the UFGs to chemical etching as a result of the higher fraction of grains and phase boundaries. The CG bands were elongated along the extrusion direction and had a relatively large aspect ratio. It is believed that the elongated CG bands and the UFG zones originated from the mixed raw 2009Al powders and the milled composite powders, respectively. The milled CNT/2009Al powders underwent severe deformation during milling, resulting in significant grain refinement to form the UFG. During hot-pressing, extrusion, and heat treatment, the UFG could barely be coarsened because of the pinning effect of CNTs. As a result, the CNT-rich UFG zones were formed in the heterogeneous composites. For the mixed raw 2009Al powders, during extrusion with a large extrusion ratio of 16:1, they were deformed along the extrusion direction to form elongated CG bands. Because the concentration of the mixed raw 2009Al powders was relatively high (>20 vol%), the elongated CG bands would connect with each other during extrusion, thereby forming the CG bands with very large aspect ratios in the heterogeneous composites. Furthermore, the composites fabricated by mixing different-sized Al powders had three different widths of the CG bands. This means that heterogeneous composites with ultra-narrow (Fig. 2(a)), narrow (Fig. 2(b)), and wide CG bands (Fig. 2(c)) were successfully achieved.

Fig. 3 shows the TEM images of typical heterogeneous 3 vol% CNT/2009Al composites (4% CNT-25% narrow CG). The grains of the CG bands were ~4 μm in size, and no CNTs were observed in the CG bands (Fig. 3(a)), while the UFG zones had a much smaller grain size of approximately 100–300 nm, even after the complicated heating history (Fig. 3(b–c)). Fig. 3(c) shows that CNTs in the UFG zones were uniformly dispersed and approximately aligned parallel to the extrusion direction. The length of CNTs was approximately 200 nm, much shorter than that of the as-received CNTs due to the severe shearing effect during milling. Nevertheless, the integrity of the tube structure was maintained well (Fig. 3(d) and (e)). Furthermore, the CNT-Al interfaces were well bonded. These results agreed well with those of our previous study [15].

Fig. 4 shows the OM and TEM images of the heterogeneous 3 vol % CNT/2009Al composites with different CG concentrations. For the 3.75% CNT-20% CG composite and the 4% CNT-25% CG composite, almost all of the CG bands were straight (Fig. 4(a) and (b)), and all of CNTs in the UFG zones were singly dispersed (Fig. 4(d) and (e)). As the CG concentration further increased to 33%, namely, the 4.5% CNT-33% CG composite, wide and nonstraight CG bands rather than narrow CG bands were mainly observed (Fig. 4(c)). In addition, some of CNT clusters appeared in the UFG zones as the local CNT concentration in the UFG zones increased to 4.5 vol% (Fig. 4(f)). To ensure a constant CNT concentration in the composites, an increase in the CG concentration led to an increase in local CNT concentration in the UFG zones, which increased the risk of CNT clustering.

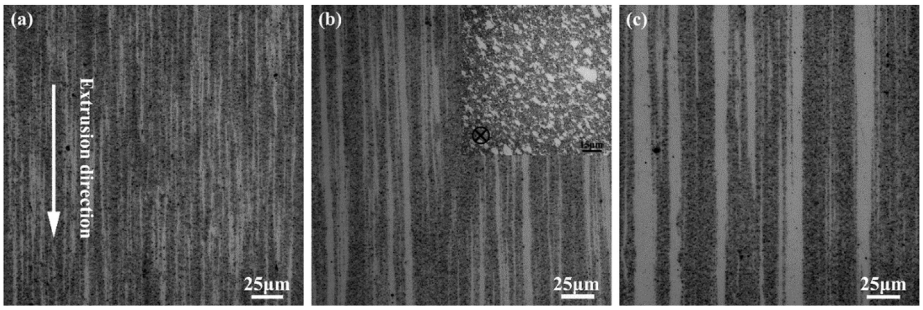

Fig. 2. OM images of heterogeneous 3 vol% CNT/2009Al composites consisting of 4% CNT-25% CG: (a) ultra-narrow CG band, (b) narrow CG (inset is OM image perpendicular to the extrusion direction) and (c) wide CG.

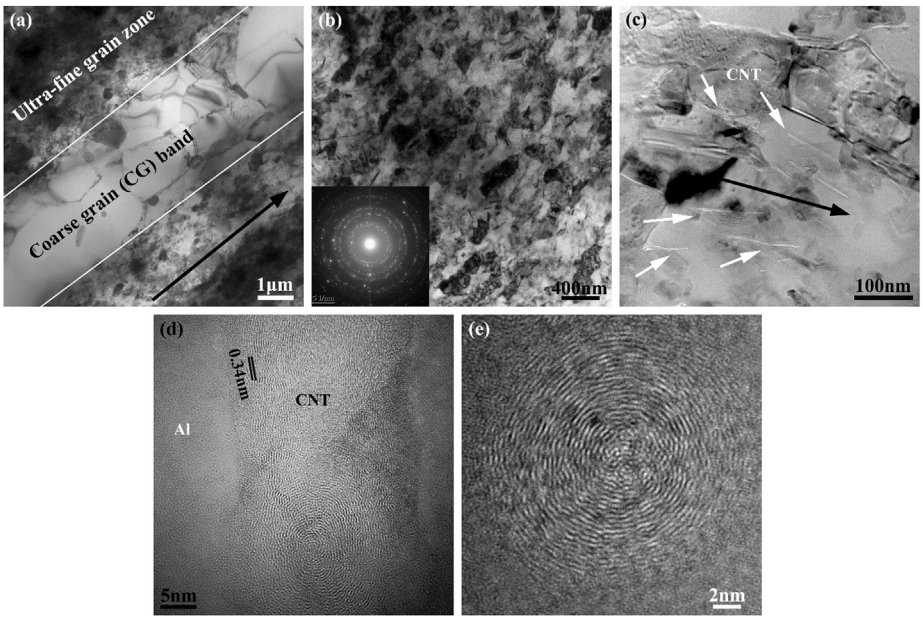

Fig. 3. (a) Typical TEM images of heterogeneous 3 vol% CNT/2009Al composites (4% CNT-25% narrow CG), (b)(c) TEM image showing grains and CNT distribution in UFG zones, and (d)(e) tube structures of CNTs in the UFG zones (black arrows indicate the extrusion direction, and white arrows denote CNTs).

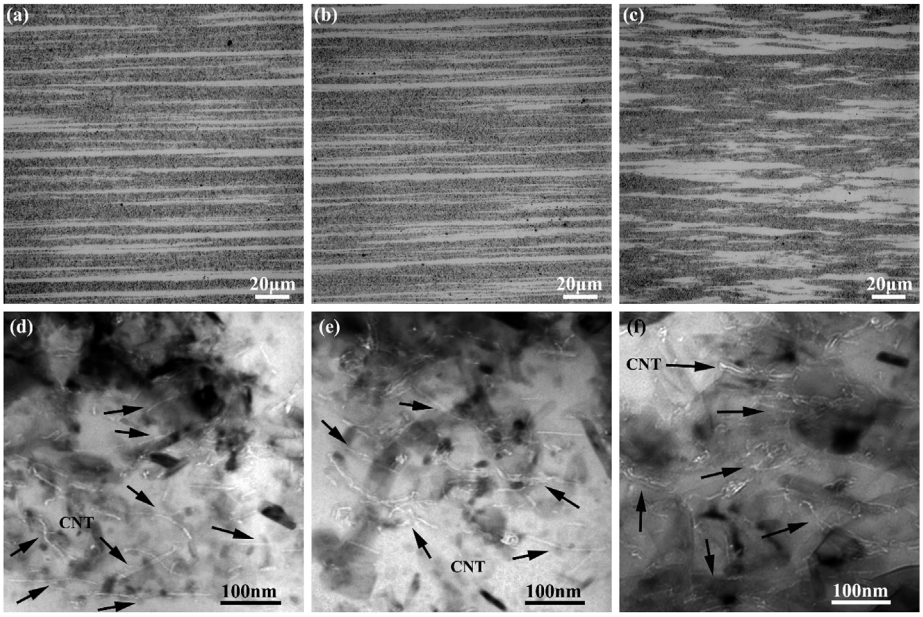

Fig. 4. OM and TEM images showing CG band distributions and UFG zones in heterogeneous 3 vol% CNT/2009Al composites with narrow CG bands: (a)(d) 3.75% CNT-20% CG, (b)(e) 4% CNT-25% CG, and (c)(f) 4.5% CNT-33% CG (black arrows denote CNTs).

Table 1
Tensile properties of heterogeneous 3 vol% CNT/2009Al composites.

Composites	YS (MPa)	UTS (MPa)	El (%)
3 vol% CNT-0%CG	703 ± 7	756 ± 11	2 ± 0.5
4.5% CNT-33% narrow CG	599 ± 9	700 ± 7	3 ± 0.5
4% CNT-25% narrow CG	610 ± 8	748 ± 10	4.5 ± 0.5
3.75% CNT-20% narrow CG	605 ± 9	690 ± 8	3 ± 0.5
4% CNT-25% wide CG	620 ± 6	714 ± 5	3 ± 0.5
4% CNT-25% ultra-narrow CG	618 ± 7	715 ± 8	2.5 ± 0.5

3.2. Tensile properties of different-structured composites

Table 1 shows the tensile properties of the heterogeneous 3 vol% CNT/2009Al composites with different CG band widths and concentrations. The uniform composites without CG addition had much higher yield strength (YS) of 703 MPa and ultimate tensile strength (UTS) of 756 MPa but lower elongation (El) of only 2%. By constructing the heterogeneous structures with 25% CG bands, although YS was slightly reduced, the elongation increased significantly. This indicates that the heterogeneous structure was beneficial to increase the ductility. For the 4% CNT-25% CG composites with different CG band widths, the strengths of the three

composites were quite similar. However, the composite with narrow CG bands had the highest elongation of approximately 4.5%. This indicates that the CG bands with a narrow width were more beneficial to improve the ductility.

Compared with the uniform composites without CGs, constructing 20% CG bands resulted in decreased strength (YS ~605 MPa, UTS ~690 MPa) but increased elongation to 3%. By increasing the CG concentration to 25%, the YS increased only a little to 610 MPa, but the UTS increased to 748 MPa and the elongation significantly increased to 4.5%. However, further increasing the CG concentration to 33% did not increase the strength and elongation further; on the contrary, both the strength and elongation were reduced. Both the highest strength and elongation were achieved for 25% CGs. The reduced strength and ductility at 33% CGs could be attributed to the high local CNT concentration of approximately 4.5 vol% in the UFG zones. This point is discussed later. These results indicate the optimized design for the heterogeneous composites can be achieved with 4 vol% CNT/2009Al as the UFG zone material and by adopting narrow CG bands with a width of ~4 μm. In the following section, the heterogeneous composites under discussion are 4% CNT-25% narrow CG composite, unless noted otherwise.

3.3. Tensile properties of optimized heterogeneous composites

Fig. 5(a) shows the tensile stress-strain curves for CG 2009Al, uniform 4 vol% CNT/2009Al, and heterogeneous composites consisting of UFG zones with 4 vol% CNT and different CG contents. The uniform 4 vol% CNT/2009Al composite showed high brittleness and rapid fracture rate after the yield stage. By introducing CG bands into the uniform 4 vol% CNT/2009Al composite, El was pronouncedly increased. An interesting phenomenon was that, by adding 25% CGs, the UTS did not reduce but was a little larger than that of the uniform composite without CGs, indicating a great toughening effect.

Tensile stress-strain curves of the 3 vol% CNT/2009Al composites are shown in Fig. 5(b). An obvious fluctuation could be observed on the tensile curve of the uniform composite. On comparison, the tensile curve for the heterogeneous composite was smoother. More importantly, the heterogeneous structure resulted in an El increment of more than twice, with nearly no UTS loss, although the YS was reduced by approximately 13% as compared to that of the uniform composite. These results indicate that the heterogeneous structure could enhance the strength-ductility of the CNT/2009Al composite effectively.

Usually, the area under stress-strain curve can be used to estimate the strength-ductility combination of a material, which can partially represent the absorbed energy during plastic deformation and crack propagation [22,30]. To simplify, in some investigations [31,32], the product of UTS and El (UTS × El) was used to represent the area. For a more accurate estimation, a modified strength-ductility product (SDP) of 0.5(YS + UTS) × El was used to calculate the area under stress-strain curve. The SDPs of the unreinforced alloy and the composites are summarized in Table 2. For the uniform composites, although the incorporation of CNTs increased the strength, the ductility decreased significantly. As a result, the uniform 3 vol% CNT/2009Al composite exhibited a much lower SDP of 14.6 MJ/m^3 than the unreinforced alloy (43.9 MJ/m^3).

For the heterogeneous 3 vol% CNT/2009Al composite, the SDP was approximately twice as that of the uniform composite. The properties of the CNT/Al composites fabricated by HEBM reported in the literature [9,12,15,33,34] are shown in Fig. 5(c) for comparison. The reported uniform composites exhibited a strength-ductility trade-off; that is, high strength was accompanied by low ductility. By contrast, the heterogeneous composites in this study showed a combination of high strength and good ductility. It was previously reported that the heterogeneous B_4C/Al composite exhibited a promoted SDP that was 1.29 times of the uniform composite [22]. By comparison, the heterogeneous CNT/2009Al composites exhibited a higher increment of SDP and El. This result is mainly attributed to the appropriate CG parameters (concentration and width) and highly efficient strengthening in the UFG zones by CNTs.

4. Discussion

4.1. Tensile behavior and deformation coordination of heterogeneous composites

A plateau on the tensile curve (also called Lüders strain) is a common phenomenon after the yield of fine-grained Al–Mg and Al–Cu–Mg alloys, and this is usually believed to be related to local deformation, attributed to the Mg solute pinning dislocations. In this study, the tensile curves of the 3 vol% CNT/2009Al composite with either a uniform or a heterogeneous structure exhibited this phenomenon, as shown in Fig. 5(b). However, the fluctuation for the uniform composite was more intense than that for the heterogeneous composite, which could be attributed to the coordination effect of CG bands.

Fig. 6(a) shows the magnified tensile curve of the heterogeneous 3 vol% CNT/2009Al composite. A sharp abnormal drop could be observed at point “b” on the curve. From OM observation of the prestretched specimen at this point, some micro-cracks initiated in the UFG zones (Fig. 6(b)). The unloading of the stress in the cracked CNT-rich UFG zones resulted in stress reduction. This could be reflected by the fracture morphology of the heterogeneous composites. As shown in Fig. 6(c), many ridge-shaped zones corresponding to the CG bands were distributed on the fracture surface. At a high magnification, small dimples were detected close to the ridge-shaped zones and the pulled-out CNTs were observed at the

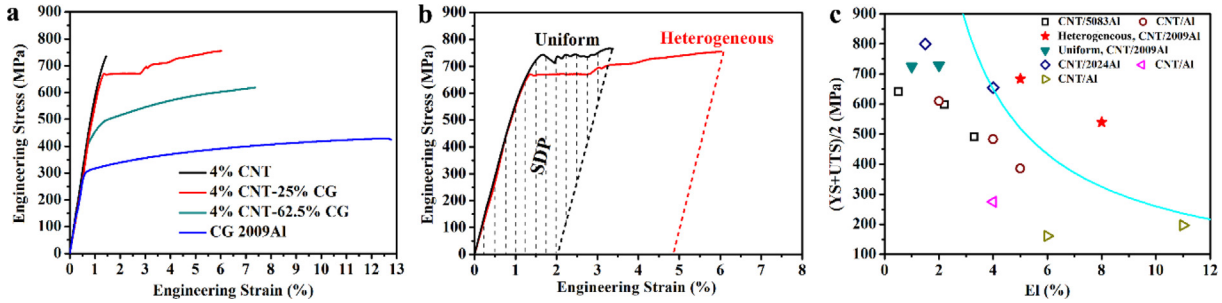

Fig. 5. Engineering stress-strain curves of (a) heterogeneous composites containing different CG contents and (b) uniform and heterogeneous 3 vol% CNT/2009Al composites; (c) strength-ductility of CNT/Al composites fabricated by HEBM [9,12,15,33,34]. (A colour version of this figure can be viewed online.)

Table 2
Tensile properties of uniform and heterogeneous CNT/2009Al composites with different CNT concentrations.

CNT	YS (MPa)	UTS (MPa)	El (%)	0.5(YS + UTS) × El (MJ/m^3)	Structure
0	305 ± 2	427 ± 3	12 ± 1	43.9	Uniform, CG
3 vol%	703 ± 7	756 ± 11	2 ± 0.5	14.6	Uniform, UFG
4 vol%	718 ± 9	732 ± 7	0.3 ± 0.2	2.2	Uniform, UFG
1.5 vol%	453 ± 3	608 ± 6	7 ± 1	37.1	[a] Heterogeneous
3 vol%	610 ± 8	748 ± 10	4.5 ± 0.5	30.6	[a] Heterogeneous

[a] Heterogeneous: Heterogeneous composites of 4% CNT-X% narrow CG.

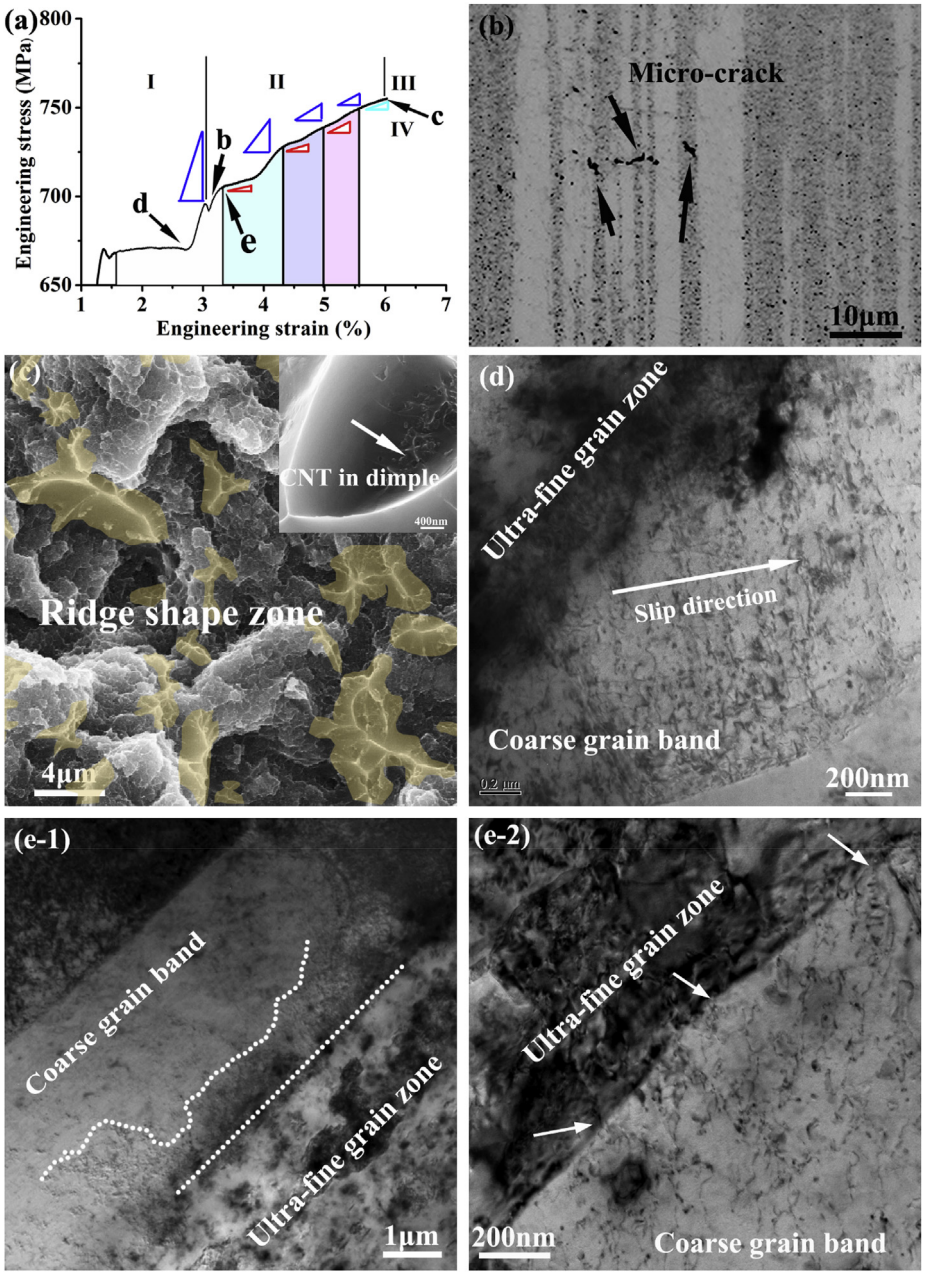

Fig. 6. (a) Locally magnified tensile curve; (b) micro-crack initiation corresponding to the tip-drop on tensile curves at point "b"; (c) fractograph (ridge-shaped zones are marked by yellow color, and the inset is a magnified view of the ridge-shaped zone boundary); and dislocations after (d) 1% plastic strain (point "d") and (e-1, e-2) 2% plastic strain (point "e") for the heterogeneous 3 vol% CNT/2009Al composite. (A colour version of this figure can be viewed online.)

bottom of the dimples (inset in Fig. 6(c)). The existence of dimples and the pull-out behavior of CNTs in the UFG zones indicate the existence of micro-void coalescence. This finding was in accordance with the result that the micro-cracks initiated at the UFG zones. It should be mentioned that no further stress drops on the tensile curve were observed (Fig. 6(b)), which implies the absence of

micro-crack propagation or further initiation during work hardening.

Furthermore, alternation of high and low work hardening rates appeared after Lüders strain (Fig. 6(a)). At the stage of Lüders strain, the two zones were considered to continue deform independently. This could be reflected by the dislocations in the CG bands for the composite pre-stretched to 1%, as shown in Fig. 6(d). Most of the dislocations were parallel to each other, and the dislocation line directions were perpendicular to the maximum shear force direction. This means that the deformation in the CG bands was mainly dominated by dislocation slip, and there was no obvious interaction between the CG and UFG zones. After the Lüders strain plateau related with the local yielding, the CNT-rich UFG zones began to deform as a whole, and thus, a high work hardening rate was achieved due to the pinning effect of the CNTs.

As the strain increased, high reacting stress was concentrated at CNTs and grain boundaries in the UFG zones, which restricted the further dislocation multiplication. As a result, the deformation was dominant in the CG bands without CNTs and a lower work hardening rate was obtained. Simultaneously, the inconsistent deformation of the CG and UFG zones increased to a critical value, and extra dislocations could be induced to relax the stress concentration. As shown in Fig. 6(e-1), large numbers of dislocations were observed in the CG band side close to the CG-UFG boundaries after pre-stretching to 2% plastic strain.

A higher magnified image (Fig. 6(e-2)) confirmed that dislocations initiated at the CG-UFG boundaries. These results suggest the formation of geometrically necessary dislocations (GNDs) due to the severe plastic deformation incompatibility of the CG and UFG zones. Once a certain number of GNDs was formed, the reacting stress concentration at the dislocation source in the CNT-rich UFG zones would be relaxed. As a result, the dislocation emission and multiplication in the CNT-rich zones started again. Then a stage with another high work hardening rate would occur. That is how the repeated stages of high and low work hardening rates could be formed. One thing should be noticed that the work hardening rate of the high work hardening rate stage decreased and that of low hardening rate stage increased with each cycle. Finally, the work hardening rates of the two different work hardening rate stages reached a similar value after several cycles (Fig. 6(a)). In this way, coordinated deformation of the heterogeneous structure was realized.

4.2. Extra strengthening of heterogeneous structure

The heterogeneous composite can be considered as an UFG (CNT/2009Al)-reinforced CG (2009Al) composite. The rule-of-mixtures was applied to calculate the strength of the heterogeneous composite:

$$\sigma_{Bi-modal} = \sigma_{CG} V_{CG} + \sigma_{UFG} V_{UFG} \quad (1)$$

where V_{CG} and V_{UFG} are the volume fractions of the CG and UFG zones, respectively; σ_{CG} and σ_{UFG} are the strengths of the CG and UFG zones, respectively. For the heterogeneous 1.5 and 3 vol% CNT/2009Al composites, their V_{CG} values were 0.625 and 0.25, respectively. As shown in Table 2, it is known that the YS of the CG bands (2009Al) and UFG zones (4 vol% CNT/2009Al) was 305 MPa and 718 MPa, respectively. Further, the UTS of the CG and UFG zones (4 vol% CNT/2009Al) were 427 MPa and 732 MPa, respectively.

As shown in Fig. 7, the calculated YS and UTS for the heterogeneous 3 vol% CNT/2009Al composite based on the rule-of-mixtures were 615 MPa and 655 MPa, respectively. The calculated YS and UTS for the heterogeneous 1.5 vol% CNT/2009Al composite were 459 MPa and 541 MPa, respectively. It is interesting to note that the calculated YS is very close to the experimental value. However, the calculated UTS is much lower than the experimental results for both the 1.5 and 3 vol% composites with the heterogeneous structure.

It was reported that gradient structure or laminate material produces an intrinsic synergetic strengthening effect, with the strength higher than the sum of the strength of separate layers, as calculated using the rule-of-mixtures [35–37]. The mechanism for this strengthening is believed to be related to the stress gradient and the complex stress state caused by mechanical incompatibility under uniaxially applied stress. For the heterogeneous CNT/Al composites, the UFG zones and CG bands could also induce severe mechanical incompatibility under applied stress, and the intrinsic synergetic strengthening effect could contribute to the strengthening. This could be verified by the formation of GNDs in Fig. 6(e1-e2).

In the early stage of plastic deformation, the deformation incompatibility between the CG and UFG zones was not obvious, and thus, the rule-of-mixtures could well estimate the YS of heterogeneous composites (Fig. 7(a)). As the plastic deformation increased, the deformation incompatibility significantly increased and large numbers of GNDs formed at the CG-UFG boundaries. These GNDs led to strong back stress strengthening in the heterogeneous composites [36], resulting in the fact that the UTS of heterogeneous composites was much higher than that predicted by the rule-of-mixtures (Fig. 7(b)).

4.3. Ductility enhancement of heterogeneous structure

For the uniform-structured composites, the elongations of the 3 and 4 vol% CNT/2009Al composites were, respectively, only 16.7% and 8.4% of that of the 2009Al alloy. The low elongation of CNT/Al composites could mainly be attributed to two reasons. First, CNTs greatly restricted the deformation of the Al matrix, and this was a common phenomenon for discontinuously reinforced metal matrix composites [38]. Second, CNT incorporation led to much finer grain size with a low dislocation storage capacity. A certain number of CG bands in the heterogeneous composites could effectively reduce the restriction effect of CNTs and make use of the advantage of the large dislocation storage capacity.

To reveal the different strain evolutions during tensile deformation, the longitudinal strain distributions of uniform and heterogeneous composites with macroscopical strains from 0 to 3.4% were tracked, as shown in Fig. 8. For the uniform composite, there was significant strain localization (Fig. 8(a–d)), and the strain could barely be transferred to other regions, which was in accordance with the low ductility. For the heterogeneous composites, under small strain, there was also strain localization in either CG bands or UFG zones, but the dimension of the strain localization zones became small (Fig. 8(e)). Under larger strain, the local strain distribution became narrow, and the deformation of the CG bands and UFG zones was more homogeneous (Fig. 8(f–h)). This was in accordance with the Lüders strain on the tensile curves (Fig. 5(b)) and clearly demonstrated that the strain localization was alleviated by the redistribution of the strain due to CG band incorporation.

According to the void growth model of Rice and Tracey [39], the growth rate of micro-voids in the matrix can be given by

$$\frac{dR}{R} = 0.28 d\varepsilon_p \exp\left(\frac{3\sigma_m}{2\sigma_e}\right) \quad (2)$$

where R is the void radius, dR is the increment in the void radius, $d\varepsilon_p$ is the increment in plastic strain, σ_m is the hydrostatic stress, and σ_e is the effective stress.

Eq. (2) indicates that the hydrostatic stress and increment in

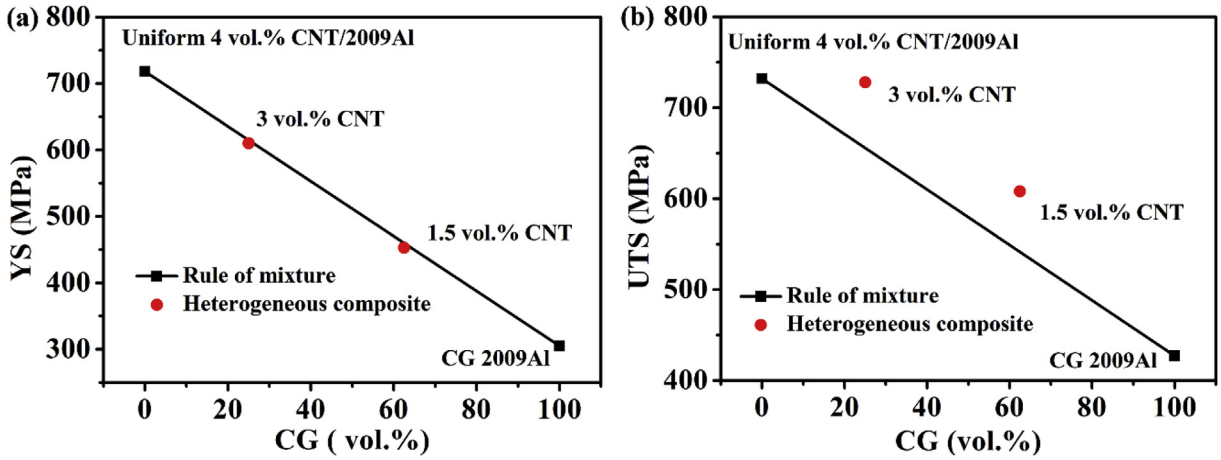

Fig. 7. Comparisons between experimental and calculated strengths of heterogeneous composites: (a) YS and (b) UTS. (A colour version of this figure can be viewed online.)

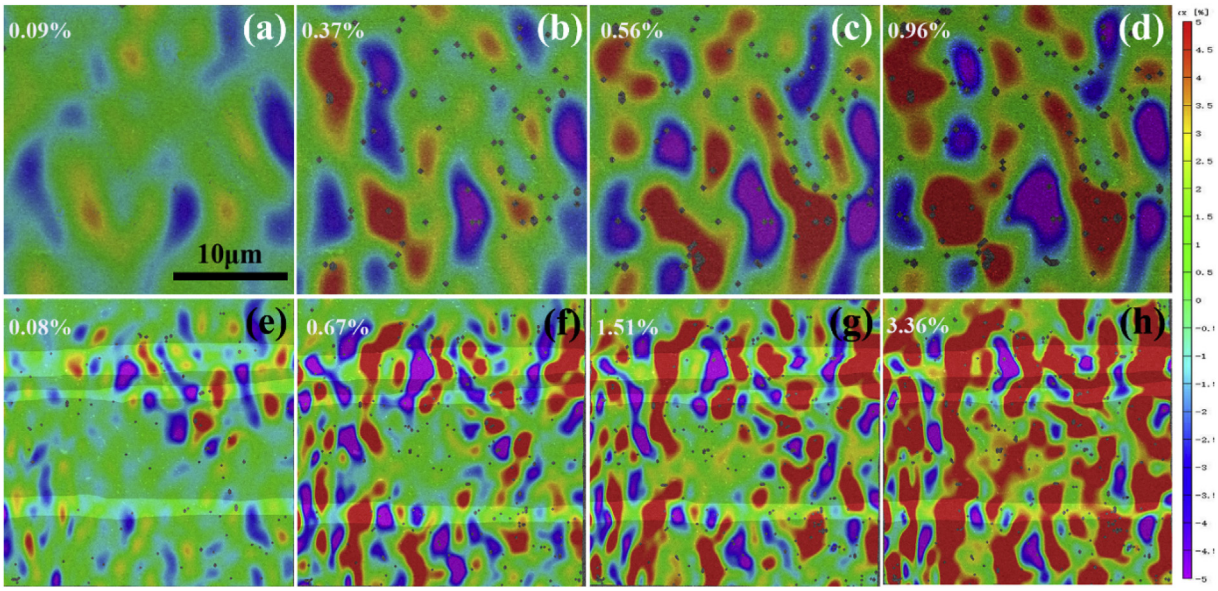

Fig. 8. Longitudinal (parallel to the tensile direction) strain distributions under different strains: (a)–(d) uniform composites with 4 vol% CNT/2009Al, (e)–(h) heterogeneous composites with 3 vol% CNT/2009Al (white zones are CG bands free of CNTs, while other zones are UFG zones containing 4 vol% CNTs). (A colour version of this figure can be viewed online.)

plastic strain have strong influences on the void growth rate. For the heterogeneous composite, strain localization is suppressed, which indicates released hydrostatic stress and smaller increment in local plastic strain in the UFG zones. According to Eq. (2), the void growth in the heterogeneous structure is greatly reduced, and thus, premature failure is suppressed.

Micro-crack blunting was another important toughening mechanism. Generally, the UFG zones stabilized by CNTs had lower dislocation storage capacity, leading to lower strain hardening. In addition, the stress concentration was induced at the CNT-Al interfaces and grain boundaries by non-compatibility of deformation during tension. Once stress increased to a critical value, micro-cracks initiated and then propagated quickly. This was evidenced in a prestretched specimen as shown in Fig. 6(b).

In the heterogeneous structure, the CG bands without CNTs were uniformly distributed in the CNT-rich UFG zones. Although micro-cracks initiated at some local sites of the UFG zones, these cracks could be blunted due to the plastic zone formation in the CG bands. As shown in Fig. 9(a), an XFEM model was built to show the crack blunting effect of CG bands in the heterogeneous composite. A preexisting crack was embedded in the UFG zones, and a tensile strain of 0.75% was applied on this model. Fig. 9(b) and (c) show the crack development in the heterogeneous and uniform composites, respectively. It indicates that the stress concentration zone in the heterogeneous composite was much smaller than that in the uniform composite. Furthermore, under the same overall strain, the crack in the uniform composite propagated to a much longer distance, while that in the heterogeneous composite was still restricted outside the CG band. It is obvious that the CG band resisted the crack development.

As discussed above, the schematic of strength-ductility enhancement for the heterogeneous composite is shown in Fig. 10. At stage I, strain localization was greatly suppressed, which is attributed to the stress redistribution for the heterogeneous structure. Therefore, the micro-void coalescence and premature initiation of micro-cracks in the UFG zones were avoided. At stage

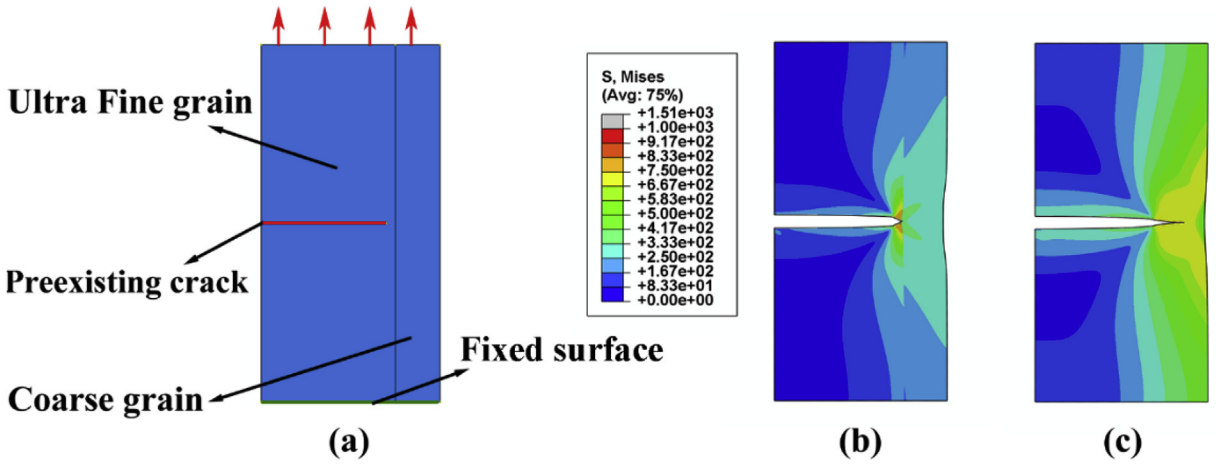

Fig. 9. (a) XFEM model for crack development in the heterogeneous material under the same strain. Local stress results of (b) heterogeneous composite, and (c) uniform 4 vol% CNT/2009Al composite. (A colour version of this figure can be viewed online.)

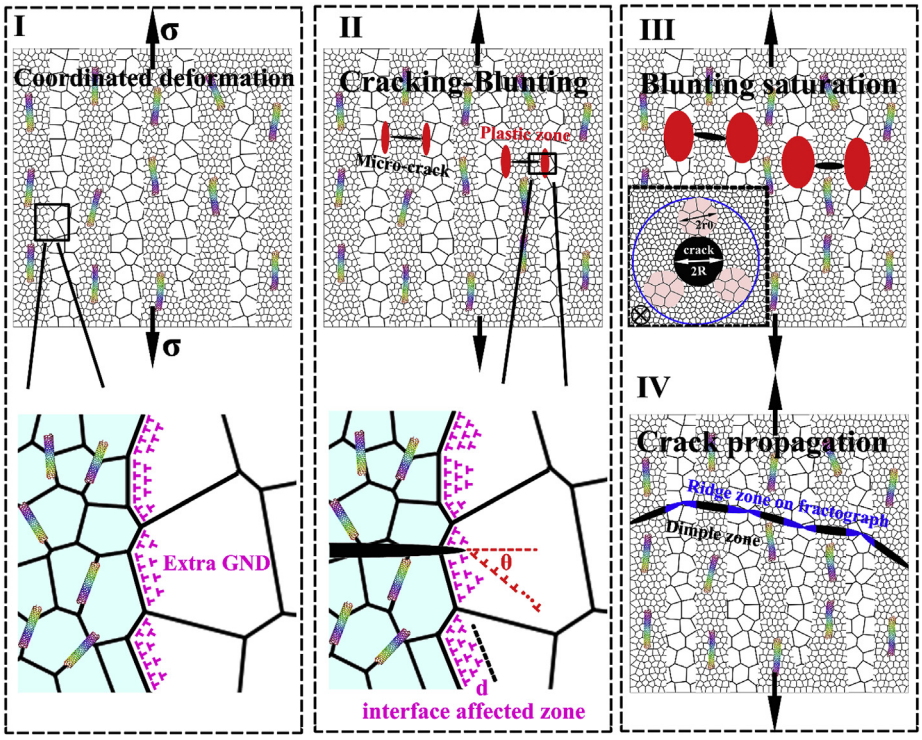

Fig. 10. Schematic of toughening mechanism in heterogeneous composites (inset in III is a view parallel to the extrusion direction). (A colour version of this figure can be viewed online.)

II, although some micro-cracks initiated in some UFG zones, they were blunted due to the formation of a plastic zone in the CG bands with the micro-mechanism of dislocation emission from crack tips. It should be mentioned that no further stress drops were found after the tip drop at point "b" in Fig. 6(a). This means that the formed cracks did not propagate, and the micro-crack re-initiation at higher strain was not significant. It also verified the perfect blunting effect of the heterogeneous structure. As the strain further increased, the plastic zones near the crack tips were saturated at stage III. Then, the micro-cracks began to propagate quickly through the entire specimen at stage IV. On the other hand, the process of deformation coordination created a large number of GNDs, according to the previous discussion. The extra GNDs led to the extra strengthening. In this way, the strength-ductility of the heterogeneous composites was effectively enhanced.

4.4. Design of CG band and local CNT concentration

Compared with wide or ultra-narrow CG bands, narrow CG bands were beneficial in increasing the strength-ductility of the heterogeneous composites (Table 2). As discussed above, the CNT-rich UFG zones had a much lower ductility, and micro-cracks easily formed in these zones. This means that the UFG zone width among the CG bands could be regarded as micro-crack length, 2*R*.

Assuming that a micro-crack forms, propagates to the CG-UFG

boundaries, and is affected by the "plastic zone" around the crack tip (inset in Fig. 10, stage III), the embedded circle crack will not propagate when the stress intensity factor is lower than fracture toughness, that is,

$$K = \frac{\sigma_0\sqrt{\pi R}}{\frac{\pi}{2}} < K_{IC} \tag{3}$$

where K is the stress intensity factor, K_{IC} is the fracture toughness of the heterogeneous composite, and σ_0 is the stress imposed on the composite. If the interaction between the two zones in the heterogeneous composite is neglected, the fracture toughness of the heterogeneous composite can be expressed as

$$K_{IC} = V_{CG}K_{IC}^{CG} + (1 - V_{CG})K_{IC}^{UFG} \approx V_{CG}K_{IC}^{CG} \tag{4}$$

where K_{IC}^{CG} and K_{IC}^{UFG} are the fracture toughness of CG and UFG zone materials, respectively. Considering the much lower strength-ductility of the UFG zone material (namely, the uniform 4 vol% CNT/2009Al), the fracture toughness of the UFG zone material can be neglected. Therefore, Eq. (3) can be changed to

$$K = \frac{2\sigma_0}{\pi V_{CG}}\sqrt{\pi R} < K_{IC}^{CG} \tag{5}$$

By substituting the concentration of CG bands $V_{CG} = \frac{\frac{\pi}{2}(r_0)^2}{\frac{3\sqrt{3}}{4}(r_0+R)^2}$ in Eq. (5), we obtain

$$K = \frac{2\sigma_0}{\pi V_{CG}}\sqrt{\pi r_0\left(\sqrt{\frac{2\pi}{3\sqrt{3}V_{CG}}} - 1\right)} < K_{IC}^{CG} \tag{6}$$

where r_0 is the average half width of the CG bands. Eq. (6) demonstrates that increased CG content and reduced width of the CG bands are beneficial to blunt the crack. On the other hand, the width of the CG bands should be larger than that of the plastic zone size.

$$r_0 > r_p = \frac{1}{2\sqrt{2}\pi}\left(\frac{K}{\sigma_{CG}}\right)^2 = \frac{\sqrt{2}R}{\pi^2}\left(\frac{\sigma_0}{\sigma_{CG}}\right)^2 = \frac{\sqrt{2}r_0\left(\sqrt{\frac{2\pi}{3\sqrt{3}V_{CG}}} - 1\right)}{\pi^2}\left(\frac{\sigma_0}{\sigma_{CG}}\right)^2 \tag{7}$$

Eq. (7) can be modified to

$$V_{CG} > \frac{2\pi}{3\sqrt{3}\left[1 + \frac{\pi^2}{\sqrt{2}}\left(\frac{\sigma_{CG}}{\sigma_0}\right)^2\right]^2} \tag{8}$$

It should be pointed out that extremely fine CG bands are not good for toughening. As discussed above, GNDs form at the CG boundaries. The reaction stress field due to the interface GNDs will restrict the dislocation emission of the micro-crack tip, which will reduce the blunting effect. According to the finding of Zhu et al. [40], the GND width, namely, the interface-affected zone in the CG bands, can be calculated using the equation

$$d \approx \left(\frac{G}{\sigma}\right)^2 b \tag{9}$$

where d is the GND width in the CG bands, G is the shear modulus, b is Burgers Vector, and σ is the strength of CG bands. To effectively blunt the micro-crack, the half width of the CG bands should be

$$r_0 > d \approx \left(\frac{G}{\sigma}\right)^2 b \tag{10}$$

For the 2009Al CG band, G is approximately 27 GPa, b is 0.286 nm, and σ is 425 MPa. After substituting these values in Eq. (9), the GND width is determined to be approximately 1.2 μm. This value is in agreement with the result shown in Fig. 6(e1). For the heterogeneous composite with ultra-narrow CG bands, its CG bandwidth is approximately 2 μm (Fig. 2(a)), which means that all of the CG bands are affected by GNDs. This will increase the difficulty for dislocation emission during plastic zone formation due to the reacting stress of GNDs, which is harmful to the blunting effect. For the above two reasons, higher strength-ductility is achieved for the composites with narrow CG bands (width ~4 μm), rather than the composites with wide or ultra-narrow CG bands. The calculated safety zones for CG parameter design based on Eqs. (6), (8) and (10) were also determined for comparing with the experimental results of heterogeneous materials [22,41,42], and the results are shown in Fig. 11. It can be found that the calculated safety zones are in accordance with the experimental results.

Although introducing the CG bands will lead to increased strength-ductility according to Eqs. (6) and (8), the local CNT concentration in the UFG zones should be carefully controlled. As shown in Table 2, for the heterogeneous 3 vol% CNT/2009Al composites, the best strength-ductility is achieved at 4 vol% CNT-25% CG composite. On the one hand, the CG bands can provide higher dislocation storability and relax the stress concentration in the UFG zones through the blunting mechanism, thereby effectively improving the ductility. Thus, as the CG concentration increases from 0 to 25%, the elongation of the composite also increases. On the other hand, increasing the CG concentration indicates higher local CNT concentration in the UFG zones because the nominal CNT concentration is 3 vol%. The higher local reinforcement concentration leads to early micro-crack initiation for the UFG zone materials, which can be analyzed as follows.

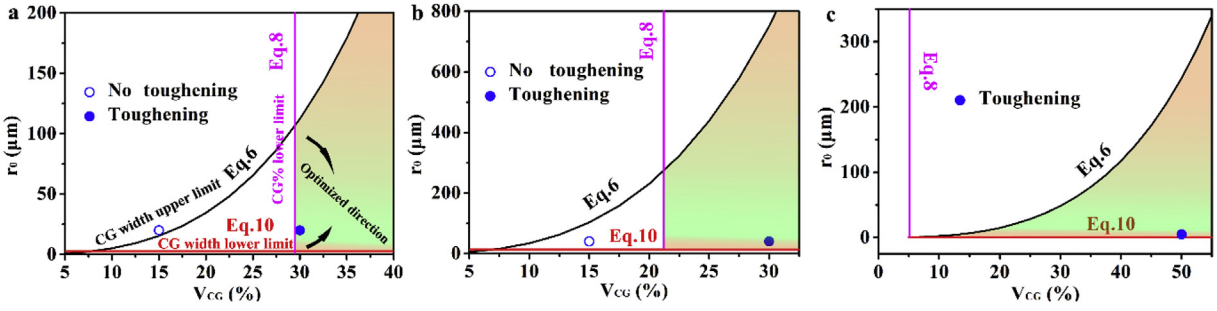

Fig. 11. Comparisons of calculated safety zones and experimental results for heterogeneous materials in Refs. [22,41,42]. (color regions are the calculated safety zones for CG parameter selection). (A colour version of this figure can be viewed online.)

Using the critical strain criterion that fracture occurs when the accumulated strain ahead of the crack tip reaches a critical value, the fracture toughness equation for particle reinforced metal matrix composites can be written as [43].

$$K_{IC} = 0.77\left\{\frac{\sigma_y \alpha \beta D_p E}{1-\nu^2}\right\} V_f^{-1/6} \quad (11)$$

where α and β are constants, ν is the Poisson ratio, V_f is the particle volume fraction, and D_p is the particle size. Eq. (11) suggests that there is a significant influence of local CNT concentration on the toughness of the UFG zones. Local CNT concentration increase indicates lower toughness for the UFG zones, and this problem is even worse as the CNT clusters appear at higher local CNT concentration (Fig. 4(g)). Furthermore, many narrow CG bands merge into wide CG bands at a higher CG concentration of 33% (Fig. 4(c)), which is also not beneficial to the strength-ductility increase.

5. Conclusions

The work outlined in this paper has shown:

(1) CNT/2009Al composites with a heterogeneous structure consisting of CNT-free CG bands and CNT-rich UFG zones were successfully fabricated using HEBM combined with powder metallurgy. CNTs with good structure integrity were dispersed in the UFG zones with grain sizes of ~100–300 nm, while the CG bands were aligned along the extruding direction with grain sizes of ~1–3 μm.
(2) Alternation of high and low work hardening rates was observed for the tensile curve of the heterogeneous composites, which could be attributed to the deformation coordination of CNT-free CG bands and CNT-rich UFG zones.
(3) The elongation of the heterogeneous 3 vol% CNT/2009Al composite increased from 2% to 4.5% while the UTS showed nearly no loss as compared to those of the uniform composite. The back stress strengthening contributed to the extra strengthening, while the strain localization suppressing and micro-crack blunting significantly enhanced ductility.
(4) Narrow CG bands rather than wide or ultra-narrow CG bands were beneficial to toughening because of the effective micro-crack blunting effect. With the same nominal CNT concentration, too many or too few CG bands were not beneficial to the strength-ductility enhancement of the composites, which is attributed to the lower toughness of the UFG zones and insufficient blunting effect of the CG bands, respectively.
(5) A model based on crack blunting was proposed for assisting the heterogeneous structure design, including the width and minimum content of CG bands. The calculated safety zones for CG parameter selection were in well agreement with the experimental results.

Declaration of competing interest

The authors declare that they have no known competing financial interests or personal relationships that could have appeared to influence the work reported in this paper.

Acknowledgments

The authors gratefully acknowledge the support of (a) Key Research Program of Frontier Sciences, CAS (No. QYZDJ-SSW-JSC015); National Key R&D Program of China (No. 2017YFB0703104), (b) the National Natural Science Foundation of China (No. 51931009, No. 51871215).

Appendix A. Supplementary data

Supplementary data to this article can be found online at https://doi.org/10.1016/j.carbon.2019.10.080.

References

[1] X. Chen, J. Tao, Y. Liu, R. Bao, F. Li, C. Li, et al., Interface interaction and synergistic strengthening behavior in pure copper matrix composites reinforced with functionalized carbon nanotube-graphene hybrids, Carbon 146 (2019) 736–755.
[2] S.R. Bakshi, A. Agarwal, An analysis of the factors affecting strengthening in carbon nanotube reinforced aluminum composites, Carbon 49 (2) (2011) 533–544.
[3] Z.Y. Liu, B.L. Xiao, W.G. Wang, Z.Y. Ma, Tensile strength and electrical conductivity of carbon nanotube reinforced aluminum matrix composites fabricated by powder metallurgy combined with friction stir processing, J. Mater. Sci. Technol. 30 (7) (2014) 649–655.
[4] J. Jafari, M.K.B. Givi, M. Barmouz, Mechanical and microstructural characterization of Cu/CNT nanocomposite layers fabricated via friction stir processing, Int. J. Adv. Manuf. Technol. 78 (1–4) (2015) 199–209.
[5] Z.Y. Liu, B.L. Xiao, W.G. Wang, Z.Y. Ma, Effect of carbon nanotube orientation on mechanical properties and thermal expansion coefficient of carbon nanotube-reinforced aluminum matrix composites, Acta Metall. Sin. 27 (5) (2014) 901–908.
[6] Z.Y. Liu, B.L. Xiao, W.G. Wang, Z.Y. Ma, Developing high-performance aluminum matrix composites with directionally aligned carbon nanotubes by combining friction stir processing and subsequent rolling, Carbon 62 (2013) 35–42.
[7] D.H. Nam, S.I. Cha, B.K. Lim, H.M. Park, D.S. Han, S.H. Hong, Synergistic strengthening by load transfer mechanism and grain refinement of CNT/Al–Cu composites, Carbon 50 (7) (2012) 2417–2423.
[8] Z.Y. Liu, B.L. Xiao, W.G. Wang, Z.Y. Ma, Elevated temperature tensile properties and thermal expansion of CNT/2009Al composites, Compos. Sci. Technol. 72 (15) (2012) 1826–1833.
[9] H. Choi, J. Shin, B. Min, J. Park, D. Bae, Reinforcing effects of carbon nanotubes in structural aluminum matrix nanocomposites, J. Mater. Res. 24 (8) (2009) 2610–2616.
[10] S.J. Xu, B.L. Xiao, Z.Y. Liu, W.G. Wang, Z.Y. Ma, Microstructures and mechanical properties of CNT/Al composites fabricated by high energy ball milling method, Acta Metall. Sin. 48 (7) (2012) 882–888.
[11] J. Stein, B. Lenczowski, N. Fréty, E. Anglaret, Mechanical reinforcement of a high-performance aluminium alloy AA5083 with homogeneously dispersed multi-walled carbon nanotubes, Carbon 50 (6) (2012) 2264–2272.
[12] Z.Y. Liu, S.J. Xu, B.L. Xiao, P. Xue, W.G. Wang, Z.Y. Ma, Effect of ball-milling time on mechanical properties of carbon nanotubes reinforced aluminum matrix composites, Composites Part A 43 (12) (2012) 2161–2168.
[13] H.J. Choi, J.H. Shin, D.H. Bae, The effect of milling conditions on microstructures and mechanical properties of Al/MWCNT composites, Composites Part A 43 (7) (2012) 1061–1072.
[14] Z.Y. Liu, B.L. Xiao, W.G. Wang, Z.Y. Ma, Analysis of carbon nanotube shortening and composite strengthening in carbon nanotube/aluminum composites fabricated by multi-pass friction stir processing, Carbon 69 (2014) 264–274.
[15] Z.Y. Liu, B.L. Xiao, W.G. Wang, Z.Y. Ma, Modelling of carbon nanotube dispersion and strengthening mechanisms in Al matrix composites prepared by high energy ball milling-powder metallurgy method, Composites Part A 94 (2017) 189–198.
[16] G. Fan, Y. Jiang, Z. Tan, Q. Guo, D.B. Xiong, Y. Su, et al., Enhanced interfacial bonding and mechanical properties in CNT/Al composites fabricated by flake powder metallurgy, Carbon 130 (2018) 333–339.
[17] W. Zhou, G. Yamamoto, Y. Fan, H. Kwon, T. Hashida, A. Kawasaki, In-situ characterization of interfacial shear strength in multi-walled carbon nanotube reinforced aluminum matrix composites, Carbon 106 (2016) 37–47.
[18] B. Chen, J. Shen, X. Ye, H. Imai, M. Takahashi, K. Kondoh, Solid-state interfacial reaction and load transfer efficiency in carbon nanotubes (CNTs)-reinforced aluminum matrix composites, Carbon 114 (2017) 198–208.
[19] A.M.K. Esawi, N.T. Aboulkhair, Bi-modally structured pure aluminum for enhanced strength and ductility, Mater. Des. 83 (2015) 493–498.
[20] L. Jiang, K. Ma, H. Yang, M. Li, E.J. Lavernia, J.M. Schoenung, The microstructural design of Trimodal aluminum composites, JOM (J. Occup. Med.) 66 (6) (2014) 898–908.
[21] L.J. Huang, L. Geng, H.X. Peng, Microstructurally inhomogeneous composites: is a homogeneous reinforcement distribution optimal? Prog. Mater. Sci. 71 (2015) 93–168.
[22] L. Jiang, H. Yang, J.K. Yee, X. Mo, T. Topping, E.J. Lavernia, et al., Toughening of aluminum matrix nanocomposites via spatial arrays of boron carbide spherical nanoparticles, Acta Mater. 103 (2016) 128–140.
[23] A.B. Pandey, B.S. Majumdar, D.B. Miracle, Effect of aluminum particles on the fracture toughness of a 7093/SiC/15p composite, Mater. Sci. Eng. A 259 (2) (1999) 296–307.
[24] S.K. Vajpai, M. Ota, Z. Zhang, K. Ameyama, Three-dimensionally gradient harmonic structure design: an integrated approach for high performance structural materials, Mater. Res. Lett. 4 (2016) 191–197.

[25] M. Ota, T. Seo, K. Ameyama, Microstructure and mechanical properties of harmonic structure designed pure aluminum, in: The 8 th Pacific Rim International Congress on Advanced Materials and Processing, TMS: The Minearals, Metal & Materials Society, 2013, pp. 3253–3258.
[26] J. Ye, B.Q. Han, Z. Lee, B. Ahn, S.R. Nutt, J.M. Schoenung, A tri-modal aluminum based composite with super-high strength, Scr. Mater. 53 (5) (2005) 481–486.
[27] S. Wang, L.J. Huang, Q. An, L. Geng, B.X. Liu, Dramatically enhanced impact toughness of two-scale laminate-network structured composites, Mater. Des. 140 (2017) 163–171.
[28] H. Wei, Z.Q. Li, D.B. Xiong, Z. Tan, G. Fan, Z. Qin, D. Zhang, Towards strong and stiff carbon nanotube-reinforced high-strength aluminum alloy composites through a microlaminated architecture design, Scr. Mater. 75 (2014) 30–33.
[29] E.I. Salama, A. Abbas, A.M.K. Esawi, Preparation and properties of dual-matrix carbon nanotube-reinforced aluminum composites, Composites Part A 99 (2017) 84–93.
[30] U.G.K. Wegst, H. Bai, E. Saiz, A.P. Tomsia, R.O. Ritchie, Bioinspired structural materials, Nat. Mater. 14 (1) (2015) 23–36.
[31] C. Capdevila, C. Garcia-Mateo, F.G. Caballero, C.G. de Andres, Neural network model for improvement of strength - ductility compromise in low carbon sheet steels, Mater. Sci. Technol. 22 (10) (2006) 1163–1170.
[32] L. Guangying, M. Mingtu, M. Xinping, Z. Changxu, New process of hot stamping in combination with Q-P-T treatment for higher strength-ductility auto-parts, Adv. Mater. Res. 1063 (2015) 223–231.
[33] A.M.K. Esawi, K. Morsi, A. Sayed, M. Taher, S. Lanka, The influence of carbon nanotube (CNT) morphology and diameter on the processing and properties of CNT-reinforced aluminium composites, Composites Part A 42 (3) (2011) 234–243.
[34] J. Stein, B. Lenczowski, E. Anglaret, N. Fréty, Influence of the concentration and nature of carbon nanotubes on the mechanical properties of AA5083 aluminium alloy matrix composites, Carbon 77 (2014) 44–52.
[35] X.L. Wu, P. Jiang, L. Chen, J.F. Zhang, F.P. Yuan, Y.T. Zhu, Synergetic strengthening by gradient structure, Mater. Res. Lett. 2 (2014) 185–191.
[36] X.L. Wu, P. Jiang, L. Chen, F. Yuan, Y.T. Zhu, Extraordinary strain hardening by gradient structure, PANS (Pest. Artic. News Summ.) 111 (2014) 7197–7201.
[37] M. Yang, Y. Pan, F. Yuan, Y. Zhu, X. Wu, Back stress strengthening and strain hardening in gradient structure, Mater. Res. Lett. 4 (2016) 1–7.
[38] J.M. Torralba, C.E. da Costa, F. Velasco, P/M aluminum matrix composites: an overview, J. Mater. Process. Technol. 133 (2003) 203–206.
[39] J.R. Rice, D.M. Tracey, On the ductile enlargement of voids in triaxial stress fields, J. Mech. Phys. Solids 17 (1969) 201–217.
[40] C.X. Huang, Y.F. Wang, X.L. Ma, S. Yin, H.W. Hoppel, M. Goken, X.L. Wu, H.J. Gao, Y.T. Zhu, Interface affected zone for optimal strength and ductility in heterogeneous laminate, Mater. Today 21 (2018) 713–719.
[41] D. Witkin, Z. Lee, R. Rodriguez, S. Nutt, E. Lavernia, Al-Mg alloy engineered with bimodal grain size for high strength and increased ductility, Scr. Mater. 49 (2003) 297–302.
[42] M. Shakoori Oskooie, H. Asgharzadeh, H.S. Kim, Microstructure, plastic deformation and strengthening mechanisms of an Al-Mg-Si alloy with a bimodal grain structure, J. Alloy. Comp. 632 (2015) 540–548.
[43] A.B. Pandey, B.S. Majumdar, D.B. Miracle, Effect of aluminum particles on the fracture toughness of a 7093/SiC/15p composite, Mater. Sci. Eng. A 259 (1999) 296–307.